PCCP

PAPER

Characterization of ZnO as substrate for DSSC†

Candela Mansilla Wettstein [ab] and Cristián G. Sánchez*[ab]

Cite this: *Phys. Chem. Chem. Phys.*, 2018, **20**, 21910

Received 15th March 2018,
Accepted 13th August 2018

DOI: 10.1039/c8cp01709c

rsc.li/pccp

We present a complete analysis of the photoinjection process in 3 nm spherical ZnO nanoparticles with different dyes attached to their surface. The study was carried using a TD-DFTB model to describe the quantum dynamics of charge transfer in the presence of an external time dependent electric field simulating resonant illumination. The ZnO + dye systems have been classified according to the injection process (type I and type II) that they present. In addition, the calculated charge transfer shows that many dyes present hole injection into the nanoparticle. We have classified the charge transfer into holes or electron and compare these results with the TiO_2 + dye system obtained from the literature.

1 Introduction

Obtaining new renewable and clean energy has gained special importance in recent years due to the increase in global demand and the need to reduce the environmental impact of energy production. In this regard, the conversion of solar energy into electricity is one of the most important challenges, since it has great potential to meet future energy needs from the largest renewable source: the sun.[1–3] However, there is a compromise between the efficiency in the generation of electricity with sunlight and the cost of manufacturing the devices needed for this. In this sense, third generation solar cells allow the production of electricity at a low cost that makes them competitive in the market. Dye sensitized solar cells (DSSC) have the ability to become third generation cells if the properties of nanoscale materials are used to build different technological devices.[3–6]

It is essential to study the processes by which these cells work in order to propose new methods of synthesis and implement new materials that result in an improvement in efficiency. These cells are composed of a nano-structured semiconductor film (most commonly used are TiO_2, ZnO and SnO_2) in which a dye is anchored, which can be an organic or metal complex dye. A solar photon excites an electron of the dye which is then injected into the conduction band of the semiconductor. Then the oxidized dye is reduced by a redox couple such as I^-/I_3^-. Finally, the electrolyte is regenerated in the counter electrode (generally platinum) and thus closes the circuit. One of the most important processes in these devices is the photoinjection of the electron. This process is direct (type II) if the electron is injected at the moment in which the dye absorbs a photon, *i.e.* it is injected directly from the HOMO of the dye to the semiconductor conduction band. An indirect mechanism (type I) is also possible in which the excitation occurs purely in the dye, where an electron of the HOMO is excited to the LUMO and is subsequently injected into the conduction band of the semiconductor.[2,4–11] A diagram of the operation of these cells and of the injection mechanisms are shown in Fig. 1. According to the energies of the dye states compared to those of the semiconductor, one mechanism or another was favored. In the type I process the LUMO orbital of the dye must have some degree of coupling with the conduction band of the semiconductor, while in the type II process the HOMO of the dye must be coupled to those states.[7] It is important to note that the injection process depends mainly on the dye that is anchored to the NP.

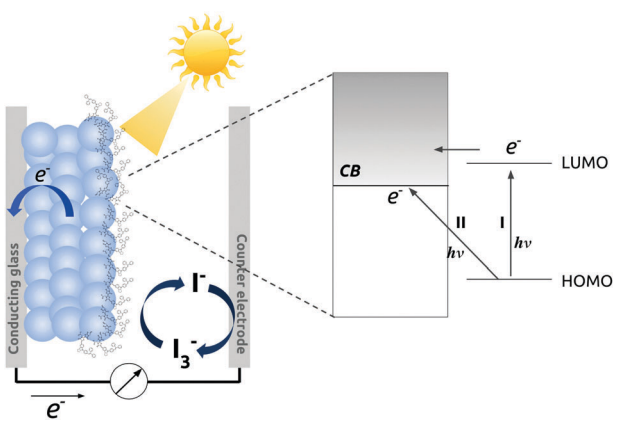

Fig. 1 Scheme of the operation of a dye sensitized solar cell.

[a] Universidad Nacional de Córdoba, Facultad de Ciencias Químicas, Departamento de Química Teórica y Computacional, Ciudad Universitaria X5000HUA, Córdoba, Argentina. E-mail: cgsanchez@fcq.unc.edu.ar

[b] Instituto de Investigaciones Fisicoquímicas de Córdoba, Consejo Nacional de Investigaciones Científicas y Técnicas (INFIQC – CONICET), Ciudad Universitaria X5000HUA, Córdoba, Argentina

† Electronic supplementary information (ESI) available. See DOI: 10.1039/c8cp01709c

This journal is © the Owner Societies 2018

Since O'regan and Grätzel report,[12] several studies were carried out about DSSCs with the aim of improving the efficiency of the cells. In particular, many investigations employed TiO_2 as semiconductor in the experiments and theoretical calculations. This is because it is a low cost, widely available and non-toxic material. Nowadays, conversion efficiencies in those DSSC reached over 10%.[9] TiO_2 (anatase) and ZnO have a similar bandgap (3.2 eV) and conduction band edge, therefore the second have seen extensively investigated to be used as DSSCs. Due to the amphoteric nature of ZnO the chemical stability is poorer than TiO_2. Nevertheless, this semiconductor has a higher electron mobility than TiO_2 and it is possible obtain a high crystalline structure (in wurtzite phase) with a wide variety of ZnO nanostructure morphologies through the use of different techniques of synthesis.[4,13] On the other hand the efficiency achieved was approximately 6.6% in those DSSC.[4]

There have been much theoretical research related to the photoinjection process in TiO_2 nanoparticles with different dyes as catechol, cresol, alizarin, coumarin, Ti(Ph-tetra-*t*Bu)-(catechol-CO_2H), 1,2-naphthalenediol, 4-nitrophenyl-acetylacetonate among others. Different methods have been used, such as DFT/TD-DFT and TD-DFTB, to study and classify the injection process that present those systems TiO_2 + dye. The analysis of the absorption spectrum, spectral bands, density of states and orbitals involved in the excitation process, have enabled a finished description of the photoinjection process and charge transfer.[7,8,14–18] However, a similar analysis for the ZnO + dye system does not exist.

In the present work, we have employed TD-DFTB calculations to study the mechanisms by which photoinjection and charge transfer occur in spherical nanoparticles of wurtzite ZnO of 3 nm of diameter, with dyes as catechol, alizarin, coumarin C343, 1,2-naphthalenediol and D149 indoline. It is well know that hierarchically structured ZnO films, that consist of spherical ZnO aggregates, improve the performance of the DSSC due to light scattering. In these systems, light these can travel large distances within the structure, enabling incident photons to be captured by dye molecules with greater probability.[19–21] It is worth noting that the method employed in these paper allows us to deal with systems of more realistic sizes than those present in the literature. The results obtained are compared with those observed in TiO_2 + dye systems. This analysis allows us to get closer to a complete description of the phenomenon of photoinjection in ZnO nanoparticles and compare it with one of the most studied semiconductors in DSSC.

2 Computational method

In this work we used a nanoparticle of 3 nm and several dyes shown in Fig. 4 for all calculations. The chosen nanoparticle size was the largest that can be simulated in a reasonable time of calculation and is composed of 1076 atoms. The nanoparticle was constructed by cutting a spherical structure from wurtzite ZnO bulk. This particle has an homogeneous distribution of O surface atoms resulting in a neutral nanoparticle. We optimized this starting geometry to minimize energy and a molecular dynamics simulation to obtain a realistic ZnO system was run, this was done within the LAMMPS code.[22] A Buckingham potential

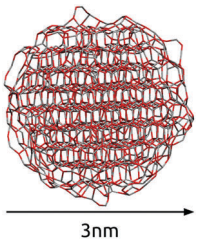

Fig. 2 Structure of Wurtzite ZnO 3 nm nanoparticle used in all electron dynamics calculations.

was been used to describe ZnO structure.[23] After energy minimization and equilibration, molecular dynamics was carried out in the canonical ensemble (*NVT*) at 300 K for 3.5 ns production runs using a time step of 3.5 fs. We chose the geometry of the last frame of this simulation for subsequent electron dynamics calculations without further optimization. This structure is show in Fig. 2. The same method for the generation of nanoparticles has been used previously by Negre *et al.*[16] (see Section S6 in the ESI† for information from the molecular dynamics). The Zn–Zn radial density function for the ZnO nanoparticle molecular dynamics and for the corresponding bulk structure are shown in Fig. 3, from this distribution it can be observed that the crystalline structure of ZnO is well conserved upon formation of the nanoparticle.

We construct the systems by adsorbing the different dyes covalently onto the nanoparticle and perpendicular to the surface of ZnO. The Zn–O arrangement that best described a tetrahedron, which is the type of arrangement found in a wurtzite hexagonal structure, was chosen as the adsorption site. Other adsorption sites were tested and shown in detail in the ESI† (Sections S3–S5). Free dyes were optimized before anchoring to the ZnO nanoparticle. Then the dye and the adjacent ZnO units to this were optimized. More about the type of bond between the Zn atom and the oxygen atoms at the adsorption site are summarized in the ESI† (see Section S1). For the optimizations we employed the DFTB+[24] code that was further used for the calculation of the electronic structure of the ground state (GS) in all systems. This code is an implementation of the self-consist-charge density-functional-tight-binding (SCC-DFTB) method[25–28] that is based on a second order expansion of the full Kohn–Sham

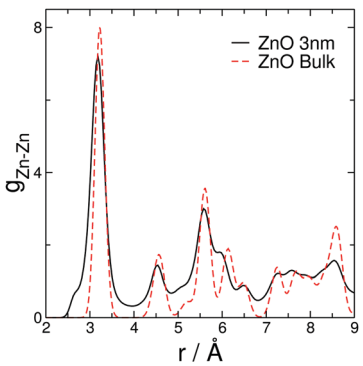

Fig. 3 Radial distribution function of wurtzite ZnO bulk and the wurtzite ZnO of 3 nm.

energy in the neighborhood of a reference density consisting of the superposition of atomic densities up to second order. This method has been successfully applied before to describe the electronic structure of large molecular system.[28,29] The DFTB+ code is used to compute the GS Hamiltonian (H_{GS}) and overlap matrix (S) and thus to obtain the initial GS reduced single-electron density matrix (ρ). The znorg-0-1[30] DFTB parameter set was employed in order to obtain the electronic structure, from which in turn the DOS and PDOS shown later where obtained.

The optical properties where calculated using a method based on the real-time propagation of the reduced single-electron density matrix (ρ) under the influence of an time-varying external potential. In this method, a delta Dirac delta pulse ($\hat{H} = \hat{H}^0 + E_0\delta(t - t_0)\hat{\mu}$) was applied to the initial ground state density matrix which is then evolved on the time according to the Liouville–von Neumann equation of motion in the non-orthogonal basis (1), which is numerically integrated. Here $\hat{H}$ denotes the hamiltonian matrix, S the overlap matrix and $\hat{\rho}$ the density matrix.

$$\frac{\partial\hat{\rho}}{\partial t} = \frac{1}{i\hbar}\left(S^{-1}\hat{H}[\rho]\rho - \rho\hat{H}H[\rho]S^{-1}\right) \quad (1)$$

This equation of motion is non-linear, since the Hamiltonian depends on the density matrix *via* the self-consistent terms and includes the same physics, albeit approximately, as the full fledged TD-DFT framework using a time local exchange correlation functional, with the advantage that it can be applied to much larger systems using relatively modest computational resources. Our implementation uses General Purpose Graphical Computing Processors (GP-GPUs) in order to accelerate the computational integration. The method has been described in detail by Oviedo *et al.*[15] and Negre *et al.*[16]

The integration of eqn (1) was performed with a 0.0005 fs time step for 20 000 steps, resulting in 100 fs of simulation. The intensity of the electric field was $E_0 = 0.001$ V Å^{-1}, ensuring that the electronic dynamics evolves within the linear response regime. The conditions for this are described in Yabana and Bertsh's work.[31] Within this regime, the temporal evolution of the density matrix is used to obtain the time dependent dipole moment, which can be calculated as shown in eqn (2).

$$\mu(t) = \int_{-\infty}^{\infty} \alpha(t-\tau)E(\tau)\mathrm{d}\tau \quad (2)$$

Here $E(\tau) = E_0\delta(\tau - t_0)$ and $\alpha(t - \tau)$ is the polarizability along the axis over which $E(t)$ is applied.

The absorption cross section is proportional to the imaginary part of the frequency dependent polarizability, therefore, we apply a Fourier transform to the eqn (2) to obtain the polarizability as a function of the energy, as shown in eqn (3). We have exponentially damped the signal with a 10 fs lifetime factor to obtain a uniform broadening of peaks and. Then the absorption spectra are calculated averaging the polarizabilities over the three cartesian directions.

$$\alpha(E) = \frac{\mu(E)}{E_0} \quad (3)$$

The charge transfer was calculated using the same method described in the previous paragraph. This method allows us to simulate the interaction of the system with an external sinusoidal electric field, in particular, a monochromatic field (*i.e.* a laser) is used. The term that is added to the Hamiltonian at each time step is $\frac{1}{2}\left(SH'(t) + H'(t)S\right)$ where $H'(t)$ is

$$\hat{H}' = -\hat{\mu}\cdot\mathbf{E}(t) = e\sum_i r_i E_i(t) \quad (4)$$

where $\hat{\mu}$ is the dipole moment, $\boldsymbol{E}(t)$ is the electric field vector, $i = x$, y, z, r_i is the position of the atom to which atomic orbital i belongs, $E_i(t) = \hat{e}_i\sin(\omega t)$, $\hat{e}_i$ is the component of the direction vector in the direction i, ω is the laser frequency and t is the time. Using a value of ω that is resonant with a certain transition it is possible to study the properties of a particular excitation. When the laser excitation in tune with a specific excitation is applied to the system, the molecular orbital populations change in the time and we can analyze in detail the nature of the excitation. This populations can be obtained by rotation of the one-electron time-dependent density matrix to the molecular orbital basis. The diagonal elements of this rotated density matrix represent instantaneous molecular orbital populations, its off-diagonal elements representing coherences between different excitations.[32]

3 Results and discussion

We have studied the mechanism of charge transfer in systems formed by a spherical nanoparticle of wurtzite ZnO of 3 nm and a several dyes anchored to the nanoparticle. The analyzed dyes are shown in Fig. 4. Alizarin, catechol and 1,2-naphthalenediol are sensitizers most commonly used in TiO_2 based DSSCs.[7,8,16,17,33] On the other hand, coumarin C343 and D149 indoline dyes have seen studied as sensitizers for both TiO_2 and ZnO DSSCs.[14,19,34–40]

Fig. 5 shows the absorption spectra of free dyes (dashed line) and those of the dyes adsorbed on nanostructure of ZnO (solid line). The strong absorption starting at 3.5 eV corresponds to the nanoparticle. Despite the fact that the Kohn–Sham gap of these particles is of about 1.9 eV (as can be appreciated in Fig. 7) the optical gap is of 3.5 eV. The spectra of NP + alizarin and NP + D149-indoline (a and b) show the same absorption bands present in the free dyes, whereas in the spectra c–e (NP + NAP, NP + catechol and NP + C343) new bands appear in comparison with the free dyes. This behavior was observed in previous studies of TiO_2 based DSSCs and is used to characterize the photoinjection process. In the type II mechanism (direct injection process) a new charge transfer band appears in the absorption spectrum, whereas no new bands are seen in the absorption spectrum of the NP + dye complexes that present type I mechanisms (indirect injection process).[7,16] In this study, we observed that alizarin and D149 indoline adsorbed in ZnO nanoparticles show characteristics of the injection process type I, and 1,2-naphthalenediol, catechol and coumarin C343 present characteristics of the injection process type II, this information is summarized in Table 1. It is worth noting that in the TiO_2 + dye systems type II injection process were observed for catechol, 1,2-naphthalenediol and D149 indoline dyes,[7,8,16,41] while for alizarin and coumarin C343 a type I injection process is observed.[7,8,14]

 This journal is © the Owner Societies 2018

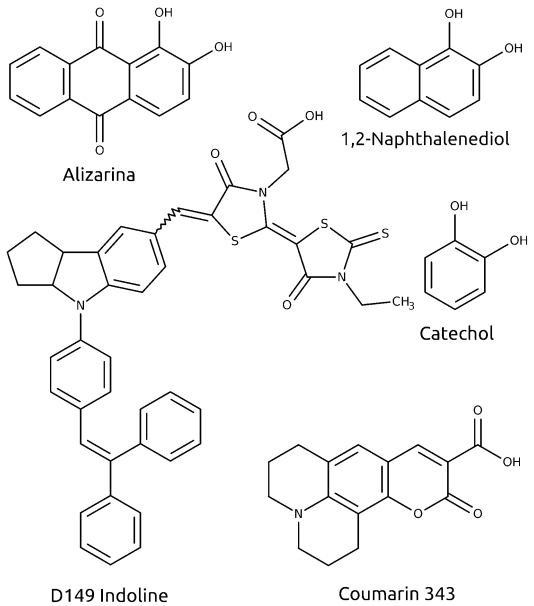

Fig. 4 Dyes used as sensitizers.

Since the maximum of solar energy distribution is in the range of 400–700 nm, we studied the lowest energy absorption band having a considerable intensity in the spectrum. These bands are indicated with an arrow in Fig. 5.

In order to study the charge transfer, a sinusoidal perturbation tuned to the energy of the peak show in Fig. 5 and in the maximal polarization direction was applied to the system NP + dye, for 100 fs. In Fig. 6 Mulliken charges *versus* time are shown. All systems present charge transfer, however, just in the NP + catechol system (Fig. 6d) electrons are transferred from dye (red line) to nanoparticle (black line). In the other systems the ZnO nanoparticle is charged positively and dye gains negative charge. Thus the dye injects holes in the nanoparticle, this behavior is summarized in the Table 2. It is worth noting that coumarin C343 anchored on a nanoparticle presents hole injection in TiO_2 as in ZnO,[42] whereas catechol inject electrons in both nanoparticles.[16]

It was observed that in 100 fs of dynamics, alizarin, coumarin C343 and D149 indoline transfer more charge to ZnO nanoparticle than the others dyes. Nevertheless, the charge transfer increases faster in ZnO + D149 indoline and ZnO + 1,2-naphthalenediol systems. Catechol and coumarin C343 inject more charge in TiO_2 during 80 fs than in ZnO nanoparticle.[16,42]

Table 1 Photoinjection mechanism observed for the different dyes studied

Type I	Type II
Alizarin	Catechol
D149 indoline	1,2-Naphthalenediol
—	Coumarin343

In Fig. 7 the total density of states of the NP + dye system (solid line) and partial density of states projected over the dye (dashed line) are shown. In systems that show hole injection (a–c and e), it is observed that dyes contribute with states in the valence band (around the edge of the valence band) of the semiconductor. Also dyes contribute with states above the Fermi energy and those are in the gap or near to the edge of the conduction band of semiconductor. This state arrangement could explain the hole injection process. When the chromophore is photoexcited an electron from the HOMO is promoted to an excited state. This electron comes from states coupled to those from semiconductor valence band as can be seen in Fig. 7a–c and e, and are promoted to the unoccupied state above the Fermi energy. This leaves a vacancy in the HOMO of dye, that is filled with electrons coming from valence band of semiconductor, leaving a hole there. In Fig. 7d catechol contributes with states above of edge of valence band and well inside of the conduction band of semiconductor. In this case, the excited electron is directly injected in the conduction band of semiconductor showing electron transfer.

At this point, it is important to clarify that these results are reproduced independently of the site in which the dye on the ZnO are adsorbed and the size of the nanoparticle. The results show that the mechanisms of photoinjection are reproducible in all cases and are presented in Sections S3–S5 of the ESI,† for dyes D149 indoline and Catechol. On the other hand, different conformations and orientations of the D149 indoline dye on the nanoparticle were analyzed, since it is the dye with the highest degrees of conformational freedom. It was possible to demonstrate that the mechanism of photoinjection is the same regardless of the conformations and orientations of the dye (see Section S2 of the ESI†).

In Fig. 8 the orbitals that involved in the excitation when illuminating the system at the energy indicated with an arrow

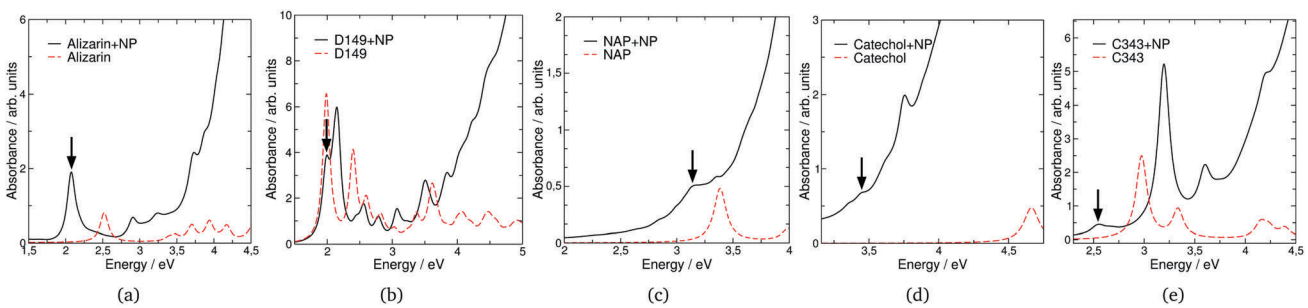

Fig. 5 Optical absorption spectra calculated for several NP + dye systems. (a) NP(ZnO) + alizarin; (b) NP(ZnO) + D149 indoline; (c) NP(ZnO) + 1,2-naphthalenediol; (d) NP(ZnO) + catechol; (e) NP(ZnO) + coumarin C343.

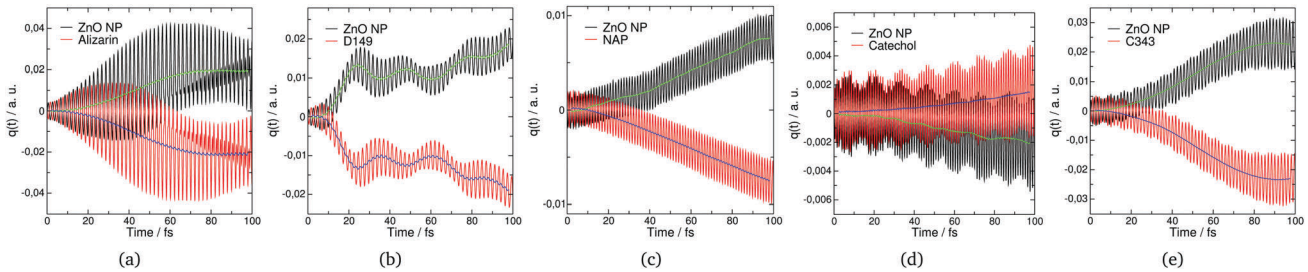

Fig. 6 Charge transfer (a) NP(ZnO) + alizarin; (b) NP(ZnO) + D149 indoline; (c) NP(ZnO) + 1,2-naphthalenediol; (d) NP(ZnO) + catechol; (e) NP(ZnO) + coumarin C343. Red lines represent the charge in the NP and black lines the charge in the dye. Green and blue lines respectively represent a running average of the charge over a laser period.

Table 2 Photoinduced charge injection of holes or electrons for the different studied dyes

Hole	Electron
Alizarin	Catechol
D149 indoline	—
1,2-Naphthalenediol	—
Coumarin343	—

in absorption spectra are plotted. In Fig. 8a the orbitals are localized on the molecule (D149 indoline), this evidences that the excitation occurs between dye orbitals, indicating a type I photoinjection. It is important to note that there is electron density over the anchor group (in the donor orbitals). After electrons are excited from the donor orbital to the acceptor orbital, the nanoparticle injects electrons to the donor orbital of the dye through this coupled state. The same behavior was observed for ZnO + alizarin (Fig. 8b), the dye is excited and then electrons flow from the nanoparticle to dye through the orbital over the anchor group, resulting in hole injection into the nanoparticle.

On the other hand, Fig. 8c shows that the orbital that is being emptied is located over the entire nanoparticle and the orbital that it is filled is localized in the dye. Hence, the photoexcitation occurs by transfer of charge directly into the NP, evidencing a type II injection process. The injection process in ZnO + catechol system (Fig. 8d) also occurs *via* an excitation of charge transfer, but in comparison with ZnO + 1,2-naphthalenediol the acceptor orbital is localized in a specific region in the nanoparticle. In this case, the dye injects electrons into the ZnO.

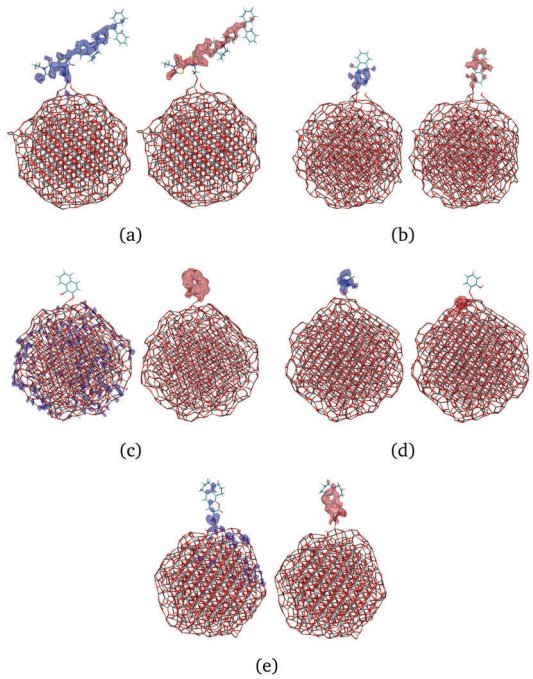

Fig. 8 Orbitals involved in the excitation of lowed energy of the spectrum. The orbital from which electrons are withdrawn is shown in blue and in red the orbital that is filled, for the following dye–NP complexes: (a) NP(ZnO) + D149 indoline; (b) NP(ZnO) + alizarin; (c) NP(ZnO) + 1,2-naphthalenediol; (d) NP(ZnO) + catechol; (e) NP(ZnO) + coumarin C343.

It is worth noting that the states near the ZnO + Dye gap play an important role in the photoinjection mechanism.

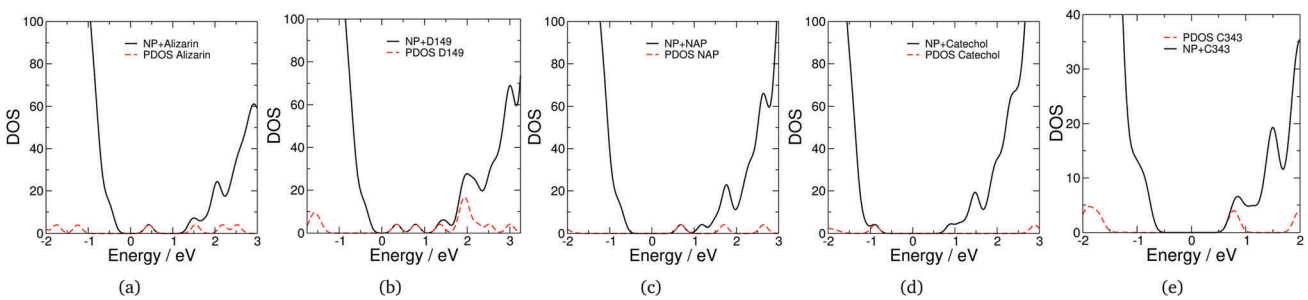

Fig. 7 Total DOS (solid line) and PDOS projected over the dye (dashed line) (a) NP(ZnO) + alizarin; (b) NP(ZnO) + D149 indoline; (c) NP(ZnO) + 1,2-naphthalenediol; (d) NP(ZnO) + catechol; (e) NP(ZnO) + coumarin C343.

 This journal is © the Owner Societies 2018

When D149-indoline dye is attached on the nanoparticle, present a gap between HOMO LUMO orbitals (of the dye) of 1.8 eV and in the case of ZnO + alizarin this gap is 1.7 eV. These states are located around the Fermi energy and are responsible for a low energy band in the spectrum.

On the other hand, catechol and 1,2-naphthalenediol present a 3.7 eV and 2.8 eV HOMO–LUMO gap respectively, they are greater than for the previous dyes, and the low energy band in the spectrum correspond to a transition between states in the nanoparticle and states in the dyes (see Fig. 7).

Even though D149-indoline and alizarin are attached to the nanoparticle by a different anchoring groups (carboxylic and catechol groups) both present type I photoinjection mechanism as explained above. Catechol and 1,2-naphthalenediol are anchored by the same group that alizarin, but in this case both ZnO + dyes complexes present a type II photoinjection mechanism, as mentioned earlier. It is worth noting that, while alizarin, 1,2-naphthalenediol and catechol have the same anchored group, the difference in the injection mechanism is given by the position of the states, where alizarin present a lower HOMO–LUMO gap than 1,2-naphthalenediol and catechol, because the resonance stabilization.

The anchoring group is not determinant of the injection mechanism, the main factor that determines this mechanism are the relative energies of the molecule HOMO and LUMO orbitals with respect to the conduction and valence bands of the particle.

A special behavior is observed for ZnO + coumarin C343 (Fig. 8e) because the orbital that is emptied is mostly on the dye but also partially localized in the nanoparticle. While the orbital that is filled is located on the dye. This system present characteristics of both injection process, which can be reflected in the absorption spectrum, where the bands of the free dye are clearly observed as in systems with type I photoinjection and a single band of lower energy similar to the observed systems that present injection of type II. This behavior was observed for TiO_2 + coumarin C343 system too.[7,18]

In previews reports it is shown that orbitals involved in the excitation of the low energy band in the spectrum for TiO_2 + 1,2-naphthalenediol are localized in the dye (HOMO) and in a specific region of the nanoparticle (LUMO) similarly to what is shown here for the ZnO + catechol complex. In this case the system injects electron into TiO_2. For TiO_2 + alizarin the injection process occur in similar way that in ZnO + alizarin and both orbitals are localized in the dye.[8]

It is worth noting that in Fig. 8c and e, the donor orbital are specifically localized over oxygen atoms in the nanoparticle. This show that the electrons of oxygen atoms are more available. The amphoteric nature of ZnO implies that nanoparticles should not be in a highly acidic or very basic medium, so that they do not dissolve.[43,44] As a consequence, there would be a greater amount of deprotonated oxygen, and the electrons of oxygen atoms are more available to be donated easily than in TiO_2 nanoparticles. It is important to point out that Ti in TiO_2 have a oxidation state of 4+, whereas Zn in ZnO is 2+. Hence ZnO nanoparticles are more capable of receiving holes compared to TiO_2. The different oxidation states of the metal in both causes a different superficial chemistry and influences the photoinduced charge transfer process.

The classification of the photoinjection processes are different for each semiconductor attached to a given dye. In TiO_2, alizarin and coumarin C343 present type I injection process, while in ZnO alizarin and D149 indoline show this process. On the other hand, catechol, 1,2-naphthalenediol and D149 indoline attached to TiO_2 show type II injection, whereas this process occurs in coumarin C343, catechol and 1,2-naphthalenediol anchored to ZnO. Differences in charge transfer were also found, observing that in ZnO most dyes inject holes into the nanoparticle, whereas only coumarin C343 does in TiO_2. On the other hand, 1,2-naphthalenediol anchored in TiO_2 injects electrons to the nanoparticle but in ZnO the same dye injects holes. These differences are related to the availability of electrons from oxygen atoms of ZnO to be donated to an orbital of the dye, while TiO_2 presents more acidic oxygens. This fundamental difference is due to the oxidation states 4+ and 2+ that Ti and Zn have in the different oxides.

4 Conclusions

In this work, ZnO was theoretically studied as a substrate for its use in DSSCs with different dyes. It could be demonstrated that it presents important differences with TiO_2 as a substrate. The injection mechanisms were determined for a range of dyes, compared to what is observed for TiO_2 and the differences related to the different chemical natures of these two oxides. In this study it was shown for several cases how it is possible to infer from the DOS whether there will be a hole or electron injection, analyzing the relative energies of the states in the Np + dye system for ZnO NPs. Summarizing, we have presented a complete analysis on the mechanisms of photoinjection in spherical ZnO nanoparticles and the comparison with TiO_2. As a future outlook we propose a more thorough exploration of the conformational space of the adsorbed dyes, at present this is unfeasible due to computational limitations.

Conflicts of interest

There are no conflicts to declare.

Acknowledgements

The authors acknowledge financial support from SeCyT UNC. This work used computational resources from CCAD – Universidad Nacional de Córdoba (http://ccad.unc.edu.ar/), in particular the Mendieta Cluster, which is part of SNCAD – MinCyT, República Argentina. CMW is grateful for a studentship from CONICET.

References

1 A. J. Nozik and J. Miller, *Chem. Rev.*, 2010, **110**, 6443–6445.
2 M. Grätzel, *Acc. Chem. Res.*, 2009, **42**, 1788–1798.
3 T. Bessho, E. Yoneda, J.-H. Yum, M. Guglielmi, I. Tavernelli, H. Imai, U. Rothlisberger, M. K. Nazeeruddin and M. Grätzel, *J. Am. Chem. Soc.*, 2009, **131**, 5930–5934.

4 A. Hagfeldt, G. Boschloo, L. Sun, L. Kloo and H. Pettersson, *Chem. Rev.*, 2010, **110**, 6595–6663.
5 M. Grätzel, *Inorg. Chem.*, 2005, **44**, 6841–6851.
6 M. Grätzel, *Nature*, 2001, **414**, 338–344.
7 R. Sánchez-deArmas, M. A. San-Miguel, J. Oviedo and J. F. Sanz, *Comput. Theor. Chem.*, 2011, **975**, 99–105.
8 M. B. Oviedo, X. Zarate, C. F. A. Negre, E. Schott, R. Arratia-Pérez and C. G. Sánchez, *J. Phys. Lett.*, 2012, **3**, 2548–2555.
9 M. Grätzel, *J. Photochem. Photobiol., C*, 2003, **4**, 145–153.
10 J. Gong, J. Liang and K. Sumathy, *Renewable Sustainable Energy Rev.*, 2012, **16**, 5848–5860.
11 A. Hagfeldt and M. Grätzel, *Acc. Chem. Res.*, 2000, **33**, 269–277.
12 B. O'Regan and M. Gratzel, *Nature*, 1991, **353**, 737–740.
13 A. B. Djurišić and Y. H. Leung, *Small*, 2006, **2**, 944–961.
14 R. Sánchez-deArmas, M. Á. San Miguel, J. Oviedo and J. F. Sanz, *Phys. Chem. Chem. Phys.*, 2012, **14**, 225–233.
15 M. B. Oviedo, C. F. A. Negre and C. G. Sánchez, *Phys. Chem. Chem. Phys.*, 2010, **12**, 6706.
16 C. F. A. Negre, V. C. Fuertes, M. B. Oviedo, F. Y. Oliva and C. G. Sánchez, *J. Phys. Chem. C*, 2012, **116**, 14748–14753.
17 W. R. Duncan and O. V. Prezhdo, *Annu. Rev. Phys. Chem.*, 2007, **58**, 143–184.
18 F. De Angelis, *Chem. Phys. Lett.*, 2010, **493**, 323–327.
19 H.-M. Cheng and W.-F. Hsieh, *Nanotechnology*, 2010, **21**, 485202.
20 T. P. Chou, Q. Zhang, G. E. Fryxell and G. Cao, *Adv. Mater.*, 2007, **19**, 2588–2592.
21 Q. Zhang, C. S. Dandeneau, X. Zhou and G. Cao, *Adv. Mater.*, 2009, **21**, 4087–4108.
22 S. Plimpton, *J. Comput. Phys.*, 1995, **117**, 1–19.
23 A. J. Kulkarni, M. Zhou and F. J. Ke, *Nanotechnology*, 2005, **16**, 2749–2756.
24 B. Aradi, B. Hourahine and T. Frauenheim, *J. Phys. Chem. A*, 2007, **111**, 5678–5684.
25 T. Frauenheim, G. Seifert, M. Elstner, T. Niehaus, C. Kohler, M. Amkreutz, M. Sternberg, Z. Hajnal, A. Di Carlo and S. Suhai, *J. Phys.: Condens. Matter*, 2001, **14**, 3015–3047.
26 M. Elstner, D. Porezag, G. Jungnickel, J. Elsner, M. Haugk, T. Frauenheim, S. Suhai and G. Seifert, *Phys. Rev. B: Condens. Matter Mater. Phys.*, 1998, **58**, 7260–7268.
27 M. Elstner and G. Seifert, *Philos. Trans. R. Soc., A*, 2014, **372**, 20120483.
28 A. S. Christensen, T. KubaÅŹ, Q. Cui and M. Elstner, *Chem. Rev.*, 2016, **116**, 5301–5337.
29 M. Gaus, Q. Cui and M. Elstner, *Wiley Interdiscip. Rev.: Comput. Mol. Sci.*, 2014, **4**, 49–61.
30 N. H. Moreira, G. Dolgonos, B. Aradi, A. L. Da Rosa and T. Frauenheim, *J. Chem. Theory Comput.*, 2009, **5**, 605–614.
31 K. Yabana and G. F. Bertsch, *Phys. Rev. B: Condens. Matter Mater. Phys.*, 1996, **54**, 4484–4487.
32 M. B. Oviedo and C. G. Sánchez, *J. Phys. Chem. A*, 2011, **115**, 12280–12285.
33 A. Nawrocka and S. Krawczyk, *J. Phys. Chem. C*, 2008, **112**, 10233–10241.
34 J. Sobuś, G. Burdziński, J. Karolczak, J. Idígoras, J. A. Anta and M. Ziółek, *Langmuir*, 2014, **30**, 2505–2512.
35 J. Xu, H. Zhang, G. Liang, L. Wang, W. Xu, W. Cui and Z. Li, *J. Serb. Chem. Soc.*, 2010, **75**, 259–269.
36 K. Hara, T. Sato, R. Katoh, A. Furube, Y. Ohga, A. Shinpo, S. Suga, K. Sayama, H. Sugihara and H. Arakawa, *J. Phys. Chem. B*, 2003, **107**, 597–606.
37 X. Liu, J. M. Cole, P. G. Waddell, T. C. Lin, J. Radia and A. Zeidler, *J. Phys. Chem. A*, 2012, **116**, 727–737.
38 J. Falgenhauer, C. Richter, H. Miura and D. Schlettwein, *ChemPhysChem*, 2012, **13**, 2893–2897.
39 A. El-Zohry, A. Orthaber and B. Zietz, *J. Phys. Chem. C*, 2012, **116**, 26144–26153.
40 T. Dentani, Y. Kubota, K. Funabiki, J. Jin, T. Yoshida, H. Minoura, H. Miura and M. Matsui, *New J. Chem.*, 2009, **33**, 93–101.
41 M. Pastore and F. D. Angelis, *ACS Nano*, 2010, **4**, 556–562.
42 C. F. A. Negre, K. J. Young, M. B. Oviedo, L. J. Allen, C. G. Sánchez, K. N. Jarzembska, J. B. Benedict, R. H. Crabtree, P. Coppens, G. W. Brudvig and V. S. Batista, *J. Am. Chem. Soc.*, 2014, **136**, 16420–16429.
43 N. Sakai, T. Miyasaka and T. N. Murakami, *J. Phys. Chem. C*, 2013, **117**, 10949–10956.
44 H. Horiuchi, R. Katoh, K. Hara, M. Yanagida, S. Murata, H. Arakawa and M. Tachiya, *J. Phys. Chem. B*, 2003, **107**, 2570–2574.

This journal is © the Owner Societies 2018